Int. J. Electrochem. Sci., 8 **(2013)** 10170 - 10189

International Journal of
ELECTROCHEMICAL
SCIENCE
www.electrochemsci.org

Effect of Conducting Salts in Ionic Liquid based Electrolytes: Viscosity, Conductivity, and Li-Ion Cell Studies

Andreas Hofmann[1,*], *Michael Schulz*[1], *Thomas Hanemann*[1,2]

[1] Karlsruher Institut für Technologie (KIT), Institut für Angewandte Materialien - Werkstoffprozesstechnik, Hermann-von-Helmholtz-Platz 1, 76344 Eggenstein-Leopoldshafen, Germany
[2] Universität Freiburg, Institut für Mikrosystemtechnik, Georges-Köhler-Allee 102, 79110 Freiburg, Germany
[*]E-mail: andreas.hofmann2@kit.edu

Received: 23 May 2013 / *Accepted:* 26 June 2013 / *Published:* 1 August 2013

A series of five conducting salts in a liquid electrolyte mixture based on propylene carbonate and N,N-diethyl-N-methyl-N-(2-methoxyethyl)ammonium bis(trifluoromethanesulfonyl)azanide is studied with respect to the usability in Li-ion cells. Namely, $LiBF_4$, $LiOSO_2CF_3$, $LiClO_4$, $LiPF_6$, and lithium bis(trifluoromethanesulfonyl)azanide are compared regarding electrochemical properties and lithium ion cell performance with respect to latest commercially available high voltage material. It is shown that an essential effect to the electrochemical performance of Li-ion based cells arises from the selection of the conducting salt. Further it is proven that reversible cycling of commercially available active materials is realizable. It is shown that coin cells work highly effective with up to date graphite anode and lithium nickel manganese cobalt oxide (NMC) cathode material using not optimized electrolyte mixtures achieving >80% of the initial discharge capacity after 400 cycles at C/10 at room temperature with ~100% cycling efficiency.

Keywords: Electrolytes, Ionic Liquids, Li-Ion-Batteries

1. INTRODUCTION

A lithium ion accumulator directly converts electrical energy and chemical energy reversibly by use of lithium ions in a chemical redox reaction. However, with respect to the high energy density in lithium ion cells, there are still challenges regarding safety, high voltage applications, and long-term stability. Therefore, a broad research on electrolytes, cathode, and anode materials is performed from numerous scientific groups and companies. Major interest lies in the study of additives to the

electrolytes which are applied for a specific and selective purpose. Numerous classes of different compounds are already identified which result in highly selective effects in a Li-ion based cell [1, 2].

Currently, ionic liquids (IL) are described as an alternative class of electrolyte solvent compounds compared to standard carbonate based systems [3]. Generally, room temperature ionic liquids (RTIL) can be considered as molten salts and be characterized by a considerably low melting point (less than 100 °C) and an almost negligible vapor pressure [4]. On the basis of these properties, ionic liquid based electrolytes are promising for safety issues in lithium accumulators [3, 5-7]. Recently, Guerfi et al. demonstrated the non-flammability of IL-carbonate-mixtures of pyrrolidinium based ILs with a content of the IL > 30% [8]. One disadvantage of pure ionic liquids is their reduced lithium ion conductivity compared to organic carbonates. However, this drawback can be overcome by the addition of selected carbonates to the ionic liquids which results in the formation of mixtures with reduced viscosity and higher conductivity retaining mainly the positive influence of the IL on safety issues [8-14].

Table 1. Conducting salts and their properties taken from Ref. [15, 16]. Anodic limit of Et_4N-X compounds in propylene carbonate (0.65 mol dm^{-3}), potential referred to Li^+/Li with a scan rate of 5 mV/s; the working electrode is glassy carbon. It should be noted that the limiting oxidation potential is here arbitrarily defined as the potential at which the current density reached 1 mA cm^{-2} at a sweep rate of 5 mV s^{-1}.

conducting salt	E_{ox} [V] vs. Li/Li^+	advantages	disadvantages
$LiPF_6$	6.8	standard conducting salt, most balanced properties [15]	thermally unstable, forms highly toxic HF with moisture
$LiOSO_2CF_3$ (= LiOTf)	6.0	thermally stable, nontoxic, insensitive to moisture	poor ion conductivity, highly corrosive to Al [15]
$LiClO_4$	6.1	economical, high anodic stability	explosive, impractical for industry purpose [17]
LiTFSA	6.3	thermally stable, safe, highly conducting	corrosive to Al (forming of $Al(TFSA)_3$) [18]
$LiBF_4$	6.6	less toxic, good electrochemical properties	hydrolysis, moderate ion conductivity, thermally unstable [15]

As mentioned by Lane et al., the organic carbonates ethylene carbonate and vinylene carbonate can significantly enhance the properties of ionic liquids for applications in lithium ion batteries [19]. Sato et al. described in 2004 that the ionic liquid N,N-**d**iethyl-N-**m**ethyl-N-(2-**m**ethoxyethyl)**a**mmonium bis(**trif**luoromethane**s**ulfonyl)**a**zanide (DMMA-TFSA) could be applied in a lithium ion based cell [12]. In this case, a high anodic stability is combined with a relatively high ionic conductivity of the pure DMMA-TFSA. However, binary mixtures of DMMA-TFSA and lithium bis(trifluoromethanesulfonyl)azanide (LiTFSA), also known as lithium bis(trifluoromethanesulfonyl)-imide (LiTFSI) [22], exhibit only a moderate reductive decomposition on the negative electrode's

active material. In a cell, the graphite surface has to be protected by a suitable additive like vinylene carbonate [12]. Recently, Le et al. studied binary LiTFSA – ammonium based ionic liquid mixtures systematically [20]. In case of using propylene carbonate (PC) in Li-ion based cells with graphite as anode material, additives have to be applied to prevent the exfoliation of graphite [21].

An essential component in a Li-ion battery is the conducting salt with respect to an accurate Li^+ transfer. Up to date, $LiPF_6$ is commonly used in Li-ion cells because of its most balanced properties regarding lithium mobility, ionic conductivity, electrochemical stability, and positive features regarding the SEI formation onto the graphite electrode. Nevertheless, $LiPF_6$ is highly toxic, moisture sensitive, decomposes to toxic products and is thermally unstable. For example it should be noted, that $LiPF_6$ shows a remarkable decomposition if the temperature exceeds 60 °C which limits the application area of Li-Ion-Batteries. Thus, alternatives are extensively investigated by academic and industrial researchers. In Table 1, selected conducting salts based on commercial availability and with good prospects for Li-ion batteries are compared. LiTFSA is described as promising material instead of $LiPF_6$. However, there are still challenges by replacing $LiPF_6$ in a Li-ion cell [23-26]. The use of lithium bis(oxalato)borate [27] is restricted in the electrolytes investigated because of its poor solubility [15, 28].

In this work we report a comprehensive study of the effects of various conducting salts in ionic liquid based electrolytes with respect to physicochemical properties and performance of Li-ion based cells. Precisely, $LiBF_4$, $LiOSO_2CF_3$, $LiClO_4$, $LiPF_6$, and LiTFSA are investigated in a DMMA-TFSA – propylene carbonate (PC) mixture from basic physico-chemical properties up to full cell studies. In order to study the properties of Li-ion cells we use graphite as anode material and NMC (lithium nickel manganese cobalt oxide, $LiNi_{1/3}Mn_{1/3}Co_{1/3}O_2$) as cathode material. NMC was chosen as a leading contender for automotive applications and PC was selected because of its significant low melting point of -49 °C in an IL-to-PC ratio of 50:50 to enhance the conductivity of the electrolyte while maintaining the safety properties of the mixtures [8]. The suitability of the mixtures regarding Li-ion based rechargeable cells is studied by measuring the specific capacity of the active material up to cell potential differences of 4.2 - 4.4 V. After presenting viscosity and conductivity data of the electrolyte mixtures, different electrode combinations, namely C|Li, NMC|Li, and NMC|C are investigated which prove the use of the electrolyte mixtures for up to date and future Li-ion battery applications.

2. EXPERIMENTAL

N,N-diethyl-N-methyl-N-(2-methoxyethyl)ammonium bis(trifluoromethanesulfonyl)azanide (DMMA-TFSA, IoLiTec, >99%), lithium bis(trifluoromethanesulfonyl)azanide (LiTFSA, IoLiTec, > 99%), and propylene carbonate (PC, Sigma-Aldrich, anhydrous, 99.7%) were dried at 110°C by means of a continuous flow of dried air. The water content of the solvents was determined by coulombmetric Karl Fischer titration to be less than 10 ppm. Vinylene carbonate (Aldrich, 97%), lithium tetrafluoroborate (Aldrich, anhydrous, 99.998% trace metals basis), lithium triflate (LiOTf, Aldrich, 99.995% trace metals basis), lithium hexafluorophosphate (ABCR, battery grade, 20 ppm H_2O max), lithium perchlorate (Aldrich, 99.99% trace metals basis), lithium foil (Alfa Aesar, 0.75 mm thick), and

hexamethyldisilazane (Aldrich, >99%) were used as received. The preparation of the electrolytes was performed in an argon-filled glove box (MBraun GmbH) with oxygen and water levels below 0.5 ppm. Calandered electrodes based on graphite and NMC with a content of approximately 90% of active material were provided in cooperation.

In this study common coin cells (type: CR 2032, Hohsen Corp.) were used with a coin cell crimper from BT Innovations. The cells were assembled in an argon-filled glove box according to standard procedures. Precisely, a graphite anode (Ø = 15 mm), a NMC cathode (Ø = 14 cm), and a glass fiber separator (Whatman®, GF/B and QMA 450; Ø =16 mm) were used inside a coin type cell with one spring and one stainless steel spacer.

The ionic conductivity of the electrolytes was measured by the standard complex impedance method, using a *Zahner Zennium IM6* electrochemical workstation in the frequency range from 1 Hz to 4 MHz. For the conductivity measurements, a Swagelok-type cell design was used by placing a PTFE ring (thickness ~ 0.35 cm) with a small hole between two stainless steel cylinders (diameter 12.7 mm). The cell assembly was done under protective atmosphere and sealed inside the glove box. The temperature dependence of the ionic conductivity was recorded by placing the test cells in a temperature and humidity chamber (*ThermoTec Espec, SH-261*). Before each measurement the cells were thermally equilibrated for at least 30 min. In the phase minimum (~ 0°) the impedance value $|\vec{Z}|$ was used for calculating the specific conductivity κ according to $\kappa = d/(A \cdot |\vec{Z}|)$ with d = length between the stainless steel electrodes and A = area inside the PTFE ring. It was found that an accurate measurement of the conductivity with this setup is realizable within a temperature range of 0 – 50 °C. Each measurement was repeated at least 3 times. The error bars include error propagation from size and values measured.

For the drying procedure and the verification of the water content a coulomb metric Karl-Fischer titration was used. The titrator consists of a *831 KF Coulometer* and a *860 KF Thermoprep* oven from Metrohm.

The cyclovoltammogramms were measured at a *Zahner XPOT* potentiostat (software: *PPSeries, Potentiostat XPot Zahner elektrik 6.4*). The potential range was 2.5 – 6 V vs. Li/Li^+ with platinum as working electrode. The cells were measured in 3-electrode configuration (EE-Cells manufactured by EL-Cell GmbH) with reference and working electrodes composed of lithium. The scan speed applied for all CV tests was 5 mV/s.

The battery tests were performed on a lithium cell cycler (LICCY, development of KIT, Institute of Data Processing and Electronics) with a maximum current of 10 mA and a voltage range of 0 – 10 V. The cut-off voltage is given in the text. The potentials reported in this paper are that of the positive electrode with respect to the counter electrode. The charging and discharging cycles were conducted with constant current based on the C-rate of the material used. Here, the calculation of the C-rate was performed in the following way: (a) [C|Li]-cells: The Cu/graphite electrode disk was weighed and the active material was calculated according to [m(overall)-m(Cu)] x 0.90. No additional correction factor for the C-rate was used. The theoretical specific capacity of the graphite used in this study is 350 mAh g^{-1}. (b) [NMC|Li]-cells: The C-rate and the cell performance were calculated based on the NMC electrode disk. In that case, the active mass of a NMC disk was calculated according to [m(overall) – m(Al)] x (active material content). The theoretical specific capacity of NMC is 278 mAh

g^{-1}, and the C-rate was calculated by using a correction factor of 0.667. This factor is justified based on the structure of NMC because a reversible insertion of Li-ions without a structural damage of NMC is only possible for some of the total Li-ions in the lattice [29]. Further, the theoretical capacity can only be obtained far beyond 4.2 V [29]. For the calculation of the [NMC|Li] performance, the active mass was used without any correction factor [29, 30]. (c) [NMC|C]-cells: The C-rates were calculated as described in (b) on the basis of NMC calculation.

Dynamic viscosity was measured using a Malvern Gemini HR Nano rotational rheometer with 40/1° cone geometry and a gap of 30 μm. These experiments were performed by using a solvent evaporation protecting cover in air. All solvents were dried carefully before the measurements and the water content was determined to be less than 10 – 20 ppm by coulomb-metric Karl Fischer titration (see above). After the measurements it was not possible to determine the water uptake because of the low solvent amount during the measurements.

The density of the electrolyte mixtures was obtained by repeated measurement of the mass of 75.0 ± 0.2 μl of an electrolyte mixture at room temperature.

Differential Scanning Calorimetry (DSC) measurements were performed at DSC 204 F1 Phoenix from Netzsch.

3. RESULTS AND DISCUSSION

3.1 Variety of the conducting salt

The chemical structures of the conducting salts, which are used in this study, are listed in Figure 1. Precisely, $LiBF_4$, LiOTf, $LiClO_4$, $LiPF_6$, and LiTFSA are investigated in battery grade quality in a mixture of PC and DMMA-TFSA. PC was used to enhance the conductivity of the mixtures with respect to an optimized cell performance while maintaining the safety issue (see also supporting information) [8]. The composition and selected properties of the mixtures are listed in Table 2.

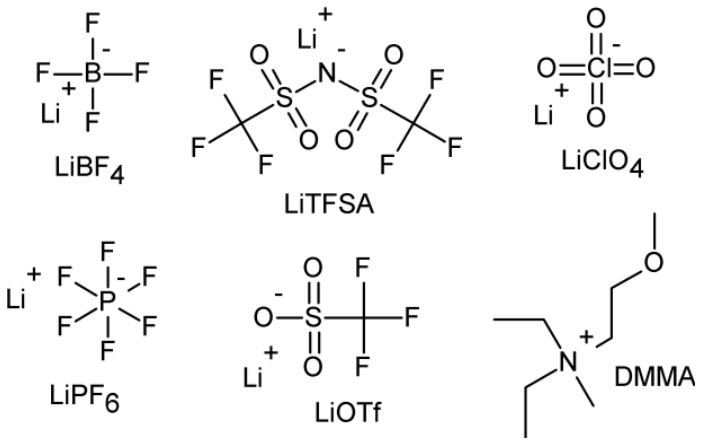

Figure 1. Structures of the conducting salts and the cation of the ionic liquid cation DMMA.

The mixtures which are used in cell studies, additionally contained selected additives, namely vinylene carbonate (VC) and hexamethyldisilazane (HMDS) (section 3.5 and 3.6). HMDS was used to remove residual traces of water and VC serves as SEI forming agent [31-36]. In mixture L-6, $LiPF_6$ serves as an additive as well because of its well-known property to protect the aluminum surface from corrosion in carbonate based electrolytes [37]. It should be mentioned that a concentration of 1 mol conducting salt in one kg of electrolyte mixture is approximately equivalent to a concentration of ~1.4 mol dm^{-3}.

Table 2. Composition and properties (ionic conductivity κ, viscosity η, and density d) at 298.15 K of the mixtures investigated.

sample	conducting salt[a,b]	solvent[b]	κ / mS cm^{-1}	η / mPa s[c]	d / g cm^{-3}
L-0	-	PC + IL	9.8 ± 0.9	7.9 ± 0.2	1.29 ± 0.02
L-1	$LiBF_4$	PC + IL	3.1 ± 0.2	39.6 ± 0.6	1.35 ± 0.02
L-2	LiOTf	PC + IL	2.3 ± 0.2	55.1 ± 0.5	1.39 ± 0.03
L-3	$LiClO_4$	PC + IL	2.2 ± 0.2	69.7 ± 1.8	1.37 ± 0.02
L-4	$LiPF_6$	PC + IL	1.9 ± 0.1	78.9 ± 4.1	1.38 ± 0.02
L-5	LiTFSA	PC + IL	1.9 ± 0.1	70.7 ± 2.2	1.44 ± 0.03
L-6	LiTFSA+$LiPF_6$	PC + IL	1.9 ± 0.1	75.9 ± 3.2	1.42 ± 0.03

[a] 1 mol conducting salt in 1 kg electrolyte mixture (L-6: 0.95 mol kg^{-1} LiTFSA + 0.05 mol $LiPF_6$). [b] IL (ionic liquid) = DMMA-TFSA; DMMA = N,N-diethyl-N-methyl-N-(2-methoxyethyl)ammonium; PC = propylene carbonate; TFSA = bis(trifluoromethanesulfonyl)azanide. Mixtures of (PC + IL) in 1:1 wt%. [c] The standard deviation signifies the distribution of the viscosity at 298.15 K within a shear rate of 10 – 200 s^{-1}.

3.2 Viscosity measurements

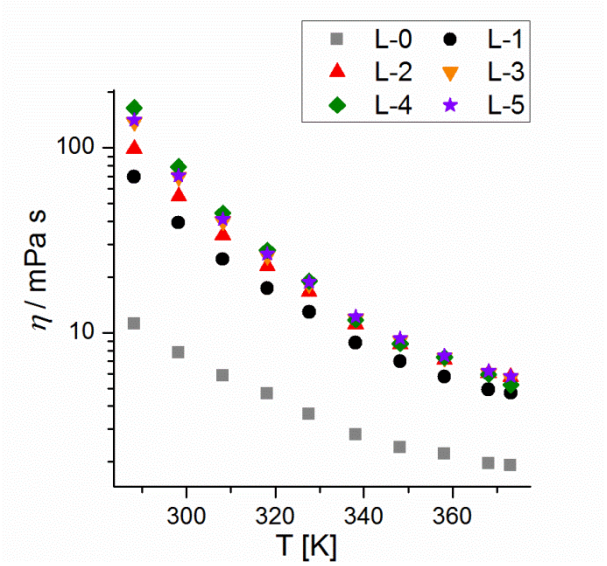

Figure 2. Viscosities of the ionic liquid based electrolyte mixtures L-*n* (*n* = 0 – 5).

The viscosity measurements of the electrolyte mixtures are depicted in Figure 2 in a temperature range of 15 – 100 °C. Mixture L-6 is not shown here because of the small difference

compared to sample L-5. The electrolytes L-3, L-4, and L-5 are quite comparable exhibiting a viscosity of ~ 73±5 mPa s at 25 °C (for comparison: pure DMMA-TFSA: 1.16 Pa·s at 25 °C, pure PC: 2.3 mPa s at 15 °C).

The addition of the conducting salt causes an increased viscosity as expected [38]. Often the empirically found Vogel-Fulcher-Tammann-Hesse [39-41] (VFTH) Equation (1) is applied for describing and characterizing the molecular motion within a liquid phase and also in battery electrolytes.

$$\eta = \eta_0 \cdot \exp\left(\frac{B}{T-T_0}\right) = \eta_0 \cdot \exp\left(\frac{D \cdot T_0}{T-T_0}\right) \quad (1)$$

η_0 is the limiting viscosity, B is a fitting parameter, D is the Angell strength parameter (see below), T_0 is the ideal glass transition temperature, and T is the absolute temperature [42, 43]. The temperature dependence of the viscosity $\eta(T)$ can be discussed based on the fragility concept according to Angell [44]. For discussing this concept, the glass-transition temperature T_g of a particular mixture has to be taken into account. The electrolytes investigated are mixtures consisting of an ionic liquid, propylene carbonate and a conducting salt and are far away being uniform pure and ideal solvents. This has to be taken into account by discussing fragility concepts which are based on a consideration of molecules in a defined phase. However, the fitting procedure according to VFTH could be applied to the electrolytes in this study with very good correlation. Usually it is recommended for an accurate data fit,[45] especially for obtaining reproducible T_0 values, to introduce an additional data point for $\eta(T_g)$ being at 10^{12} Pa·s [42, 46] or 10^{10} Pa·s [43] for more fragile compounds like ionic liquids with T_g values below room temperature. However, for the mixtures investigated, a fitting procedure is only accurate, if no additional data point at $T = T_g$ (e.g. $\eta(T_g) \equiv 10^{10}$ Pa·s) is applied and if the ideal glass transition temperature T_0 is fixed at $T_g - T_0 \equiv 30$ K [42, 45, 47, 48]. Hereby, the parameters listed in Table 3 are received from the fitting procedure with accurate R^2 values. By applying an additional data point according to literature [45], the fitting results are heavily dependent on the initializing parameters and no reliable values are received. This can be ascribed to the complexity of the electrolyte mixtures, the highly disordered solvent and salt molecules and the molecular interaction of the ionic liquid and the conducting salt. Generally it should be noted, that the fitting parameters are strongly dependent on small variations in the viscosity measurements. Therefore attention should be paid to the fact that the values obtained can only be seen as estimation. It is concluded that the liquid mixtures can be classified as *fragile* which is supported by an Angell strength parameter D of $3.3 < D < 7.4$ (fragile for $D < 30$ [44]) and the fragility factor m (steepness index [46, 49]) of $58 < m < 106$ which is in the same order of magnitude compared to the literature for ionic liquid based systems [42, 48]. Generally, the parameter D describes the "strength" of a liquid with regards to the coordination of a molecule in the liquid phase [42]. As a consequence it can be concluded based on D how closely the electrolytes obey the Arrhenius law (ideal for $D = \infty$) [44]. The values of the quotient T_g/T_0 are comparable to results described in literature for ionic liquid based systems which are in the range of 1.1 – 1.3 [42, 45, 47, 48]. Further it is concluded that the contribution of the conducting salt to the flow properties of the electrolyte mixtures is in the same order of magnitude for the investigated mixtures which is shown in the T_g scaled Arrhenius plots of the viscosities in Figure 3.

Table 3. VFTH fitting parameters for the mixtures L-*n* (*n* = 0 - 6). The glass transition Temperature T_g was obtained by DSC measurements (-150 °C – 200 °C) with a standard deviation of ± 2 K. Origin Pro 8.0 was used for the fitting procedure of the temperature dependent viscosity measurements (15 – 180 °C) and the R^2 value was better than 0.993 for all data fittings.

sample	R^2	η_0 / µPa s	B / K	T_0 / K	T_g / K	T_g/T_0	D
PC	0.993	68 ± 2	512.4 ± 9.7	154	184	1,19	3.32 ± 0.02
DMMA-TFSA	0.999	29 ± 1	1064.4 ± 10.2	161	191	1,17	6.52 ± 0.02
L-0	0.998	88 ± 7	647.6 ± 11.3	154	184	1,19	4.20 ± 0.07
L-1	0.998	38 ± 5	996.0 ± 17.8	156	186	1,19	6.40 ± 0.11
L-2	0.999	26 ± 4	1044.8 ± 15.9	156	186	1,19	6.70 ± 0.10
L-3	0.998	17 ± 3	1165.1 ± 21.5	158	188	1,19	7.36 ± 0.14
L-4	0.999	17 ± 2	1115.5 ± 16.8	166	196	1,18	6.71 ± 0.10
L-5	0.999	23 ± 4	1085.9 ± 19.3	163	193	1,18	6.64 ± 0.12

Sometimes, the Arrhenius equation (2) is applied for calculating the activation energy E_a of the flow process (viscous flow) with the universal gas constant R and the limiting viscosity η_0 [50]. However, an Arrhenius plot of the viscosity can only be analyzed and compared in small temperature ranges of some ten Kelvin.

$$\eta = \eta_0 \cdot \exp\left(\frac{E_a}{R \cdot T}\right) \tag{2}$$

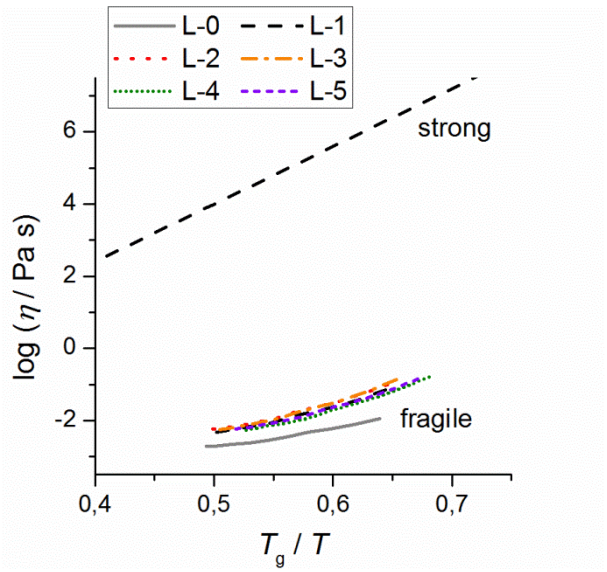

Figure 3. T_g scaled Arrhenius plots of viscosities of the ionic liquid based electrolyte mixtures L-*n* (*n* = 0 – 5). The classification is based on the Angell strength parameter *D* and the fragility factor *m*.

The Arrhenius plot and the linear fittings of the electrolytes are depicted in Figure 4 and the fitting parameters and flow activation energies are listed in Table 4 in a temperature range of 15 – 55 °C. As expected, the activation energy highly depends on the temperature range.

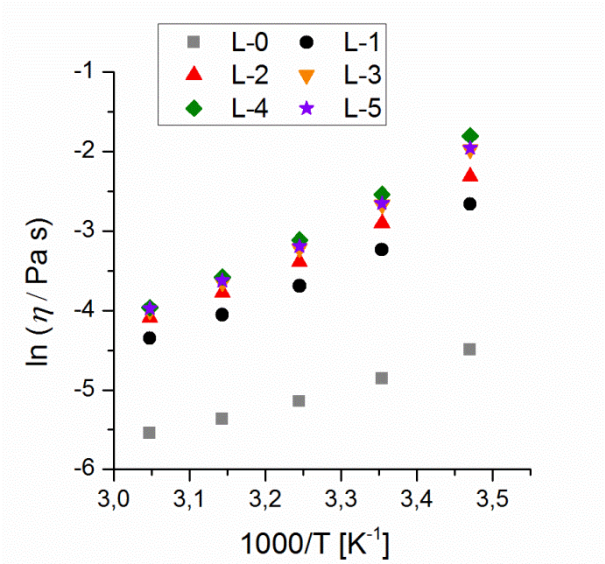

Figure 4. Arrhenius-Plot of the viscosity data of samples L-*n* (*n* = 0 – 5) with linear fittings in the range 15 – 55 °C.

Table 4. Parameters of the Arrhenius plots[a]

sample	*slope*	E_A / kJ mol^{-1}	R^2
L-0	2.48 ± 0.15	20.6 ± 0.02	0.986
L-1	3.98 ± 0.21	33.1 ± 0.01	0.989
L-2	4.21 ± 0.21	35.0 ± 0.01	0.990
L-3	4.77 ± 0.26	39.7 ± 0.03	0.988
L-4	5.09 ± 0.26	42.3 ± 0.02	0.989
L-5	4.77 ± 0.25	39.7 ± 0.02	0.988
[a] The fit procedure was done according to Equation 2.			

Comparable activation energies of 33.0 kJ mol^{-1} < E_a < 42 kJ mol^{-1} at 15 – 55 °C are obtained for the electrolyte mixtures containing conducting salt with accuracies of R^2 > 0.986 for all individual plots. Zarrougui et al. [50] have shown that the activation energy of a χ_1 = 0.47 mixture of N-butyl-N-methylpyrrolidinium TFSA and PC in a temperature range of 21 – 44 °C is 25.05 kJ mol^{-1} which fits well in the range of the data obtained for the ammonium based IL. The values indicate that an increase in the temperature causes a decrease of the energy which is necessary for the molecular motion in the electrolytes.

3.3 Conductivity of the electrolytes

The electrolyte conductivity plays a crucial role in understanding the electrochemical properties of the solvents. Therefore, the temperature dependence of the conductivity is studied and depicted in Figure 5 for the samples L-*n* (*n* = 0 – 5) in a temperature range of 5 – 45 °C. The highest conductivity exhibits the pure solvent mixture L-0. Incorporating conducting salt to liquid IL-PC mixtures reduces

the conductivity significantly by a factor of 3-5 (Figure 5). The slopes of the specific conductivities are in the same order of magnitude. A small, but significant effect of the conducting salt anion can be observed by comparing the samples L-*n* (*n* = 1 – 5). In detail, the value of the conductivity of sample L-1 is significantly higher than the values of the others. Samples L-4 and L-5 exhibit the lowest conductivity value. Nevertheless, the influence of the anion of the conducting salt to the ionic conductivity is rather small. This is quite notable since the dissociation of the conducting salt in the DMMA-TFSA/PC mixture is expected to differ. We assume that the main fractional part of the anions is delivered by the ionic liquid DMMA-TFSA ($TFSA^-$; see also Table 5) thus the conducting salt anions are presumably highly complexed by Li^+.

With increasing temperature, a rise in ionic conductivity is observed. The ionic liquid DMMA-TFSA is present in all electrolyte mixtures thus the TFSA-anion exists in all samples and is able to complex both the lithium and the DMMA cation. Additionally it is known that the Li^+ contribution to the conductivity is only a low fractional part of the total conductivity value [51]. Zarrougui et al. investigated an IL:PC (χ_1 = 0.47) mixture with the ionic liquid N-butyl-N-methylpyrrolidinium resulting in a specific conductivity of 7.84 mS/cm (at 298.15 K), which is in the same order of magnitude compared to the presented ammonium-IL:PC mixture L-0 (9.8±0.8 mS/cm at 298.15 K) [50].

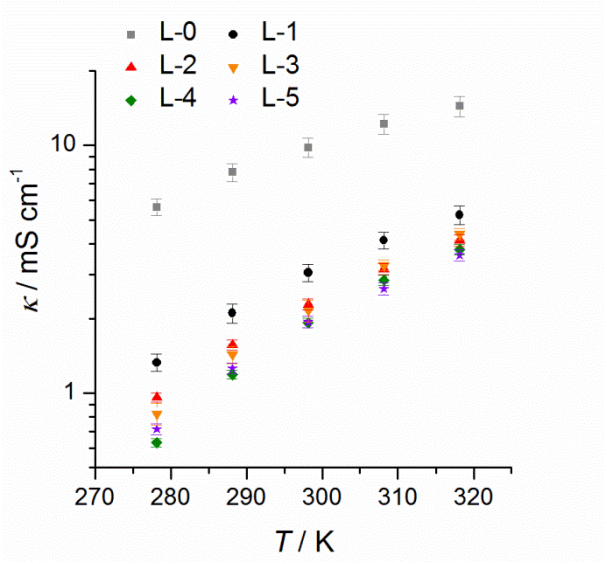

Figure 5. Ionic conductivity of the mixtures L-*n* (*n* = 0 – 5) at different temperatures. Each sample is measured at least three times independently.

It is investigated whether the mixtures obey the Walden rule [52] (Equation 3) with the limiting molar conductivity Λ_m^0 of an electrolyte and the pure solvent's viscosity η. Zarrougui et al. have shown that the viscosity and conductivity of a mixture with $\chi_1 > 0.22$ in a PC – pyrrolidinium IL mixture are closely linked thus the Walden rule could be applied [50]. A fractional Walden rule can be obtained by introducing an additional parameter *a* to the viscosity (Equation 4) which results in the linearized Equation 5 [42, 47].

$$\Lambda_m^0 \cdot \eta = C \quad (3)$$

$$\Lambda_m^0 \cdot \eta^a = C' \quad (4)$$

$$\log \Lambda_m^0 = \log C' + a \log \eta^{-1} \quad (5)$$

In this study, the limiting molar conductivity Λ_m^0 is replaced by the molar conductivity Λ_m^{cs+IL}, which consists of the amount of substance of the conducting salt (cs) n_{cs} and the contribution of the ionic liquid (IL) n_{IL} to the total molar conductivity. Thus, the ionic molar conductivity Λ_m^{cs+IL} is composed of the specific conductivity κ, the density d of the mixture and the total mass m (Equation 6).

$$\Lambda_m^{cs+IL} = \frac{\kappa}{\left(\frac{m_{cs}}{M_{cs}} + \frac{m_{IL}}{M_{IL}}\right)\frac{d}{m}} \quad (6)$$

It is found that the modified Walden rule can be applied to the highly concentrated mixtures with $c_{cs+IL} \approx 2.7 \pm 0.1$ mol dm^{-3} resulting in almost linear fits according to Equation (5) with a coefficient of determination R^2 better than 0.996. The Walden plots are depicted in Figure 6 and the parameters of the fits are listed in Table 5.

Table 5. Parameters of the Walden plots[a]

sample	c_{cs+IL} / mol l^{-1}	slope	R^2
L-0	1.58 ± 0.05	0.71 ± 0.02	0.997
L-1	2.70 ± 0.05	0.65 ± 0.01	0.999
L-2	2.69 ± 0.05	0.66 ± 0.01	0.999
L-3	2.72 ± 0.05	0.68 ± 0.03	0.996
L-4	2.70 ± 0.05	0.62 ± 0.02	0.999
L-5	2.53 ± 0.05	0.78 ± 0.02	0.998
[a] The fit procedure was done according to Equation 5.			

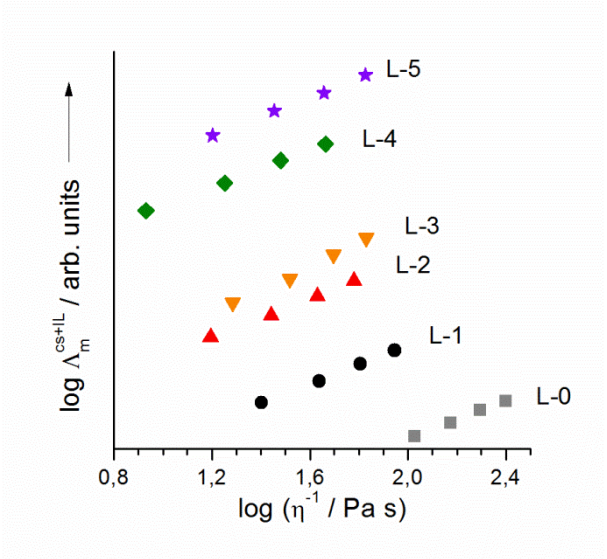

Figure 6. Walden plots of the samples L-*n* (*n* = 0 – 5). For a better comparison the plots are shifted vertically against each other.

The temperature range of the viscosity – conductivity relationship is 15 – 45 °C. This result exhibits that the empirically found Walden rule is applicable even in highly concentrated electrolytes consisting of strongly aggregated ionic liquids and conducting salts.

Closely related to the conductivity is the Li^+ transference number. Preliminary results based on pulsed field gradient NMR suggest that the Li^+ diffusion constants of the mixtures studied are in the same order of magnitude (no significant difference). Further, the Li^+ diffusion constant of the mixtures studied is lowered by a factor of ~10-20 compared to EC-DMC (1:1 wt.%) with 1 M $LiPF_6$.

3.4 Electrochemical stability

The oxidation stability of the electrolytes is tested in linear sweep voltammetry studies in Pt|Li cell configuration (three electrode configuration) and the relevant data are depicted in Figure 7. The data suggest that the mixtures exhibit an anodic stability up to a potential of 4.5 – 5.5 V vs. Li/Li^+. A significant raise in the current density arises > 5.5 V vs. Li/Li^+ only. However, it should be noted that platinum which was used as working electrode, is much more inert than aluminum or the electrode paste. Thus, it is expected that the oxidation stability is reduced in real cell configurations. It is observed that mixture L-2 exhibits a decreased stability of 4 – 4.5 V vs. Li/Li^+, which might be caused by the anion OTf^-. In contrast, mixtures L-3, L-4, and L-5 exhibit an improved anodic stability of ~5.5 V vs. Li/Li^+ compared to sample L-0.

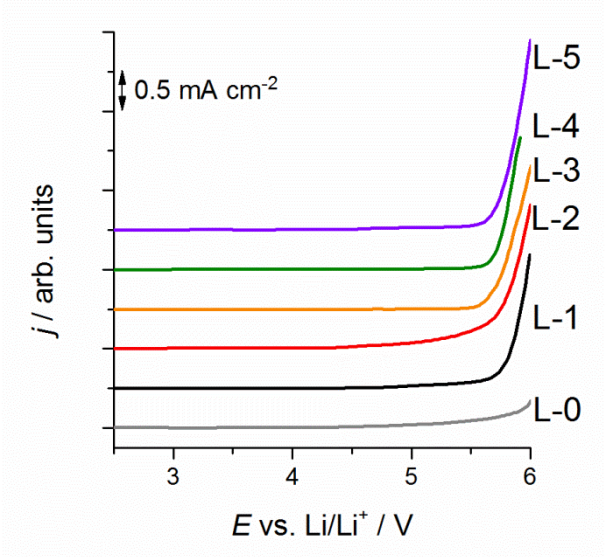

Figure 7. Linear sweep voltammetry of samples L-n (n = 0-5) with Pt as working electrode and lithium as counter and reference electrode (three electrode configuration; 5 mV s^{-1}; *E* vs. Li/Li^+ = 2.5 – 6.0 V).

3.5 C|Li and NMC|Li cell tests

The electrolyte mixtures are tested in half cell tests against lithium metal to study the performance of the samples in the presence of NMC as well as graphite. Vinylene carbonate (VC) is

used as surface electrolyte interface (SEI) forming additive for graphite in all cases in 2 wt.-% and HMDS is used as water protecting agent (0.5 wt.-%). VC plays a crucial role in forming a comprehensive layer which hampers the propylene carbonate to exfoliate the graphite in the PC/DMMA-TFSA mixtures.[12, 21] Both of the electrodes are coated and calandered in cooperation resulting in electrodes, which are proven to exhibit stable cycling in pouch cell tests for some hundreds of cycles with standard electrolyte like LP-30© (Merck, 1 M $LiPF_6$ in EC/DMC). The cells are cycled with different C-rates to enable an insight in the Li^+ transport even by applying higher charge rates. More precisely, a current rate (C-rate) of 1 C is equivalent to the current when the cell is completely charged or discharged in 1 h. The results are depicted in Figure 8. For NMC|Li cells (Figure 8a), a specific discharge capacity of 160 mAh g^{-1} is received in case of electrolyte L-1, L-3, L-4, and L-5 at C/20 reversibly, while mixture L-2 exhibits only 140 mAh g^{-1} at the beginning of the cycling.

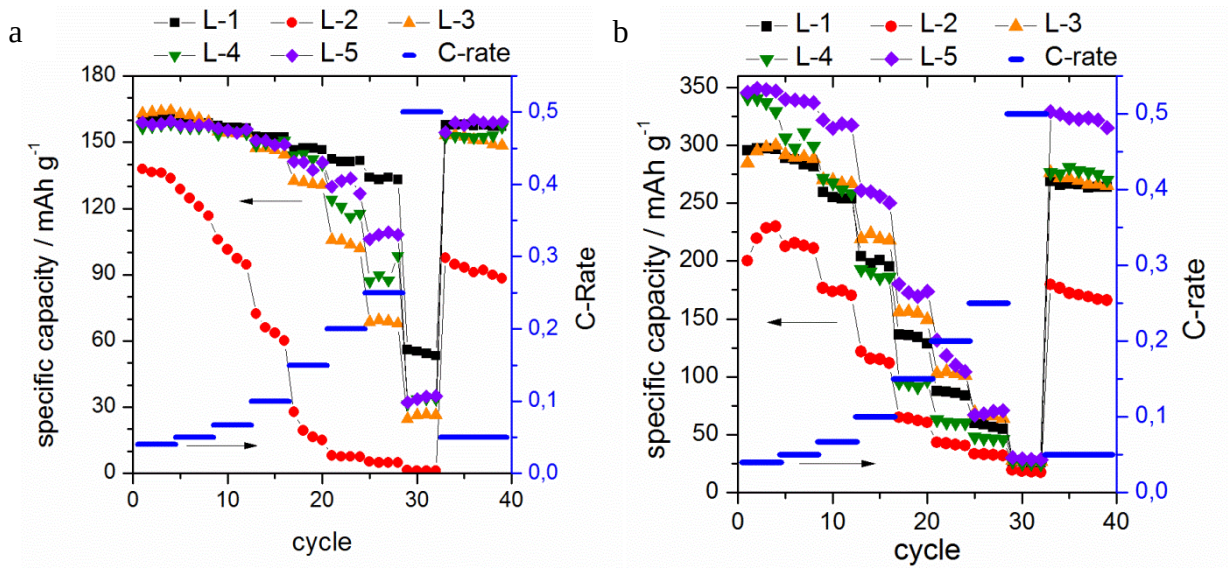

Figure 8. 8a: Discharge capacity of NMC|Li cells. Voltage range: 3 – 4.3 V. 8b: Discharge capacity of C|Li cells. Voltage range: 0 – 2 V. The electrode area is 1.267 cm^2.

Electrolyte L-2 exhibits a fast reduction of the specific capacity even in repeated measurements. In contrast, the drop of the specific capacity of the remaining mixtures with an increased charge rate is less pronounced. Nevertheless, a strong decrease of the storable energy is observed in every mixture at C/2 to a level of about 30 – 60 mAh/g. On the other hand, up to C/4, almost 135 mAh g^{-1} are obtained for the best electrolyte mixture L-1 in this test and 120 mAh g^{-1} for the LiTFSA-mixture. As a result, a conductive salt dependent behavior is observed starting from poorly working cells (LiOTf) to highly reversible cycling performance ($LiBF_4$, $LiClO_4$, $LiPF_6$, and LiTFSA). This is remarkable inasmuch as preliminary pulsed field gradient NMR (pfg-NMR) measurements reveal a comparable order of magnitude for Li-ion diffusion constants. Currently the correlation of Li-ion diffusion constants and Li^+ conductivity in IL based mixtures is systematically investigated by the authors. It is suggested that the Li^+ migration and the affinity of Li^+ to NMC is strongly dependent on the complexation of Li^+. One reason for the reduced cell performance of LiOTf

could be Al corrosion, which is known to be extraordinary strong in LiOTf mixtures [15] and which can reduce the storable energy by Al decomposition of the electrode surfaces (especially of the negative pole).

In Figure 8b, the cell configuration graphite|Li is depicted. Mixture L-1, which was one of the best electrolyte mixtures in NMC|Li cell configuration, exhibits a moderate specific capacity of 300 mAh g^{-1} at C/20. Mixture L-2 (LiOTf) reveals a reversible capacity which is ~ 200 mAh g^{-1} and thus inferior to the remaining mixtures as well. In contrast, much better results are received by using LiTFSA (L-5) and $LiPF_6$ (L-4). However, also in these cases, a rapid decrease of the specific conductivity to ~ 30 mAh g^{-1} at C/2 is obtained. Insofar it is unlikely to obtain much better specific capacities in full NMC|C cells (see below) at high C-rates. Furthermore, it is quite difficult to fully charge the graphite electrodes galvanostatically because of change in the potential towards lithium deposition [53]. If slow cycles are applied after fast cycling most of the initial capacity is retained thus an effective protection of the graphite electrodes via a solid electrolyte interface is assumed. The charge and discharge profiles of the C|Li cells are depicted in Figure 9 for a better understanding of the processes during the formation of the SEI in the first and the second cycle. No PC intercalation is observed in the range of 0.8 – 1.1 V in the potential profiles in Figure 9a [54]. Electrolyte mixtures L-4 and L-5 exhibit a fast drop of the potential down to 0.2 V with forming of the SEI in the range of 0.90 – 0.20 V.

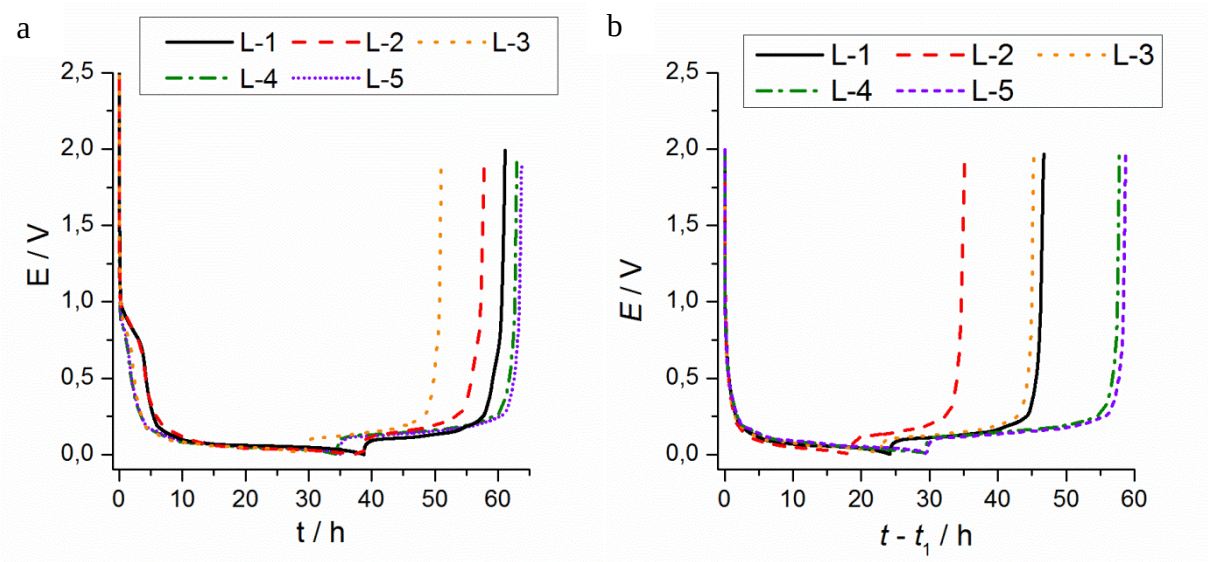

Figure 9. 9a: First charge and discharge cycle of the electrolyte mixtures at C/25 (room temperature). 9b: Second charge and discharge cycle of the electrolyte mixtures L-1 to L-5 at C/25 (room temperature) in C|Li cells. t_1 indicates the time at the end of the first cycle thus the time t at beginning of the second cycle is set to zero for a better comparison. The electrode area is 1.267 cm^2.

Below 0.2 V, a reversible Li intercalation (e.g. in L-5) can be observed clearly with a retention of 85.8% of the energy in the first cycle (U = 0.17 V at t = 4 h to U = 0.26 V at t = 63.8 h) and 99.2% in the second cycle (full cycle). In general, the different stages of Li_xC intercalation are forming below

0.25 V vs Li/Li^+ [53]. Not optimized electrolyte mixtures can be one reason for observing relatively large irreversible capacities during the first cycle. Additionally, the irreversible capacity loss in the first cycle can be attributed to SEI formation processes. Broader peaks during the SEI formation are observed for electrolyte L-2 and L-3. The shifts in the ~0.6–0.8 V range can be attributed to solvent reduction (PC and ammonium IL cation) which are only present in the first lithiation step of the graphite based on the SEI formation [55]. It is suggested that different potential curves of the electrolyte mixtures L-1 to L-5 can be observed due to different SEI formation processes. By comparing the data for the first and the second cycle (Figure 9a and 9b), it is obvious that most of the formation processes of the SEI are already completed after the first cycle. This can be attributed to the abrupt potential drop up to U = 0.18 V in the second cycles. In this study, only 2 wt% of VC is applied to the electrolytes. As a result, a content of 2 wt% of VC should be sufficient in the studied electrolyte mixtures for forming a stable SEI layer and enabling a reversible cell cycling.

3.6 NMC|C cell tests

Full cell studies in NMC|C cell configuration are performed for evaluating the electrolyte mixtures in combined electrode systems (Figure 10). The specific capacities of NMC at various C-rates during the cycling of the cells are shown in Figure 10a. Only mixtures L-3, L-4, and L-5 exhibit a cell performance which is suitable for reversible cycling. From Figure 10a and 10b it can be seen, that mixture L-1 results in only poor working NMC|C cells in contrast to X|Li cells (Figure 8). One reason might be that a large irreversible loss of Li hampers the use of $LiBF_4$ effectively. Strong corrosion effects (aluminum corrosion) of mixture L-2 can be an explanation of the poor working mixture L-2, which result in Al layer decomposition and the deposition of Al onto the C electrode [15]. At constant rates of C/20 (Figure 10b) the mixtures L-3 ($LiClO_4$), L-4 ($LiPF_6$), and L-5 (LiTFSA) exhibit the best performance. The slight decrease of the capacity after the initial cycles can be ascribed to the Swagelok like cell design and an elimination of lithium into the SEI layer (irreversible capacity) due to a not-optimized additive mixture.

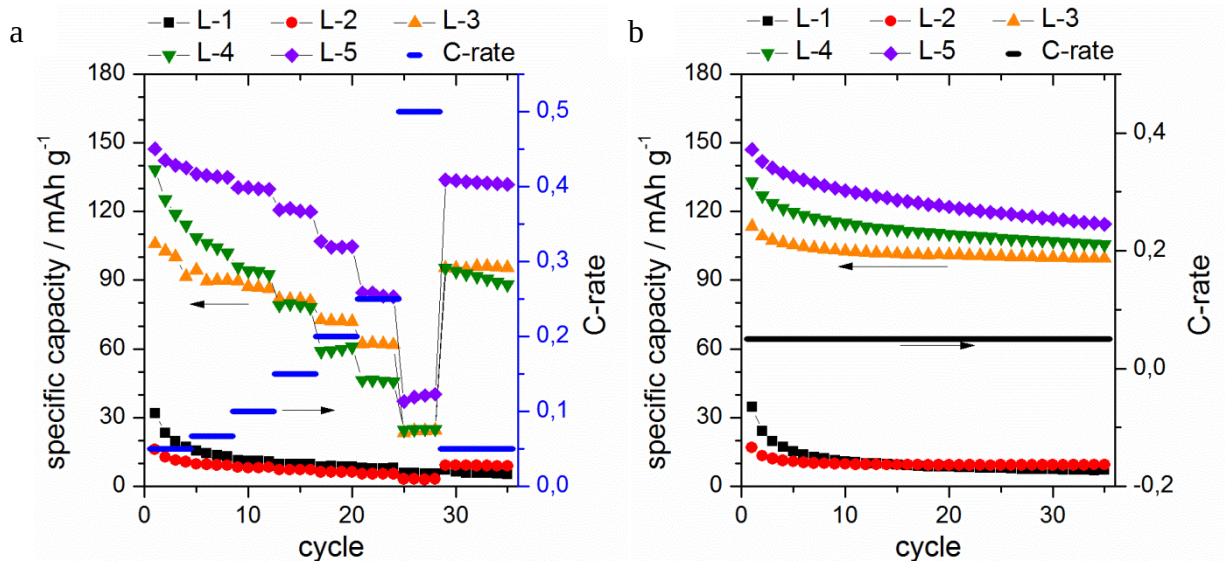

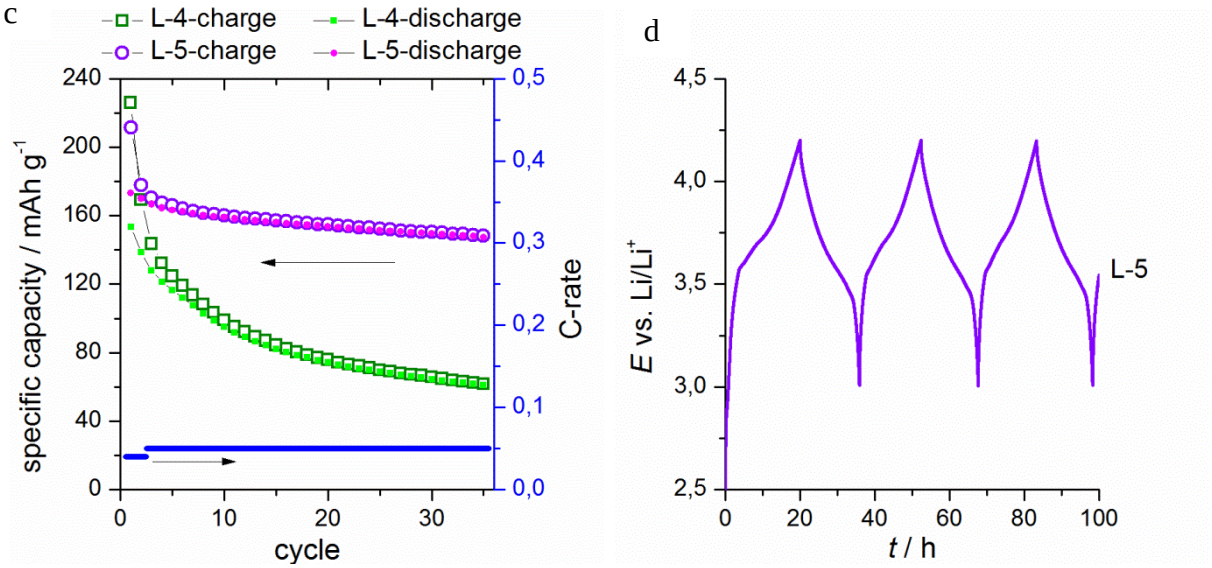

Figure 10. *Figure 10a*: Discharge capacity of NMC|C (C/20 – C/2; room temperature; E = 3 – 4.2 vs. Li/Li^+). *Figure 10b:* Discharge capacity of NMC|C cells (C/20; room temperature; E = 3 – 4.2 V vs. Li/Li^+). *Figure 10c:* Specific capacity of NMC|C cells (C/25-C/20; room temperature; E = 3 – 4.4 V vs. Li/Li^+). *Figure 10d:* Charge and discharge cycle of the electrolyte mixture L-5 at C/20 (room temperature).

By comparing C|Li- (Figure 8, right) and NMC|Li-cells (Figure 8, left) a slight decrease in the specific capacity is observed. Thus, the drop of the capacity is likely related to the graphite electrode.

Based on Figure 8 it is not clear why the electrolyte mixtures L-1 and L-2 result in not-working NMC|C-cell systems even at low current rates because the current is calculated based on the specific capacity of NMC. This means that enough graphite should be present in the cell for a working cell system. However, the low specific capacity of mixture L-1 and L-2 is reproducible and can be also seen in Figure 10.

The differences between L-4 ($LiPF_6$) and L-5 (LiTFSA) are particularly evident in Figure 10c. Here, the cut off voltage is set to be 4.4 V, thus a higher potential is seen by the electrolyte in the cell. It is remarkable that mixture L-5 retains the capacity quite well (88% based on the third cycle, 35 cycles), whereas mixture L-4 exhibits a relatively strong decrease of the specific capacity (48% based on the third cycle, 35 cycles). This is likely due to a better electrochemical stability of the $TFSA^-$ ion compared to the PF_6^- ion in the 4.2 – 4.4 potential range. In Fig 10d the charge and discharge profiles of mixture L-5 is depicted in detail. It is seen that no plateau like in $LiFePO_4$ cathode material [56] is observed but rather a gentle decrease of the specific capacity takes place with a medium discharge plateau around 3.6 ± 0.2 V. This behavior is typical for NMC material [29]. As a consequence, it cannot be deduced that electrolyte compositions that exhibit outstanding properties in X|Li half cells (compare Figure 8) perform in a similar way in full cells with graphite. It is concluded that mixture L-5 (LiTFSA in DMMA-TFSA + PC) exhibits the best cell performance in NMC|C cells. Further it indicates that the development of new electrodes requires a careful design of the electrolyte mixtures because of the interaction between both materials in a working battery cell.

To demonstrate the use of the ionic liquid based electrolyte, mixture L-6 is used in a coin cell type CR 2032 configuration. Here, $LiPF_6$ is used as additive in 1 wt% concentration in addition to VC and HMDS as a fluorine source to increase the corrosion stability against the Al current collector. The cycling profile is depicted in Figure 11a for 400 cycles and the cycling efficiency, namely the quotient of the discharge capacity and the charge capacity, is illustrated in Figure 11b.

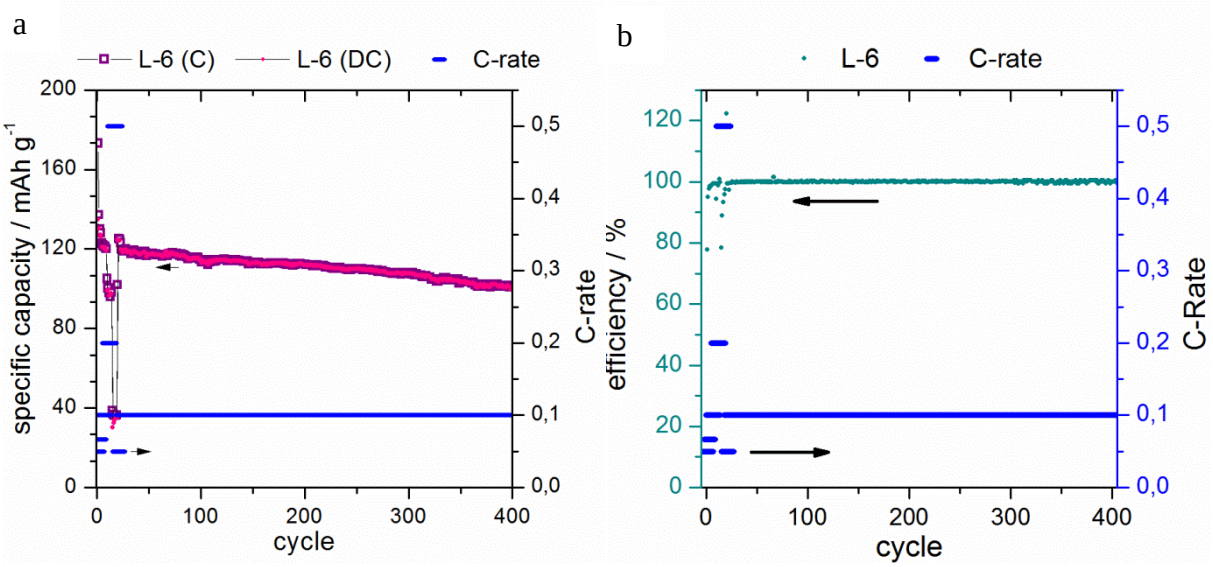

Figure 11. 11a: Charge (C) and discharge (DC) capacities of a NMC|C cell at room temperature (U = 3 – 4.2 V). The cell is performed as coin cell. Repeated measurements reveal a similar behavior. 11b: Efficiency of the NMC|C cell with electrolyte L-6 (compare Fig 6) at defined C-rates. At a constant C-rate of C/10 100% efficiency (discharge capacity / charge capacity) are obtained.

After the initial forming steps at low C-rates of C/20 and C/15, a short performance test up to C/2 is performed. A significant decrease in the specific capacity of the active material is observed while increasing the C-rate as expected from the previous measurements. However, the NMC|C-cell exhibits retention of the specific capacity of ~95% (C/10) after 120 cycles based on the fifth discharge cycle (also at C/10). After approximately 400 cycles (C/10, room temperature, coin cell), ~80% retention of the specific capacity based on the fifth discharge cycle was obtained. The cycling efficiency exhibits a retention of nearly 100% at C/10 for 400 cycles. In this context it should be noted, that the mixture L-6 is still not a fully optimized electrolyte mixture. Figure 12 highlights the temperature dependence of the mixture L-6 at 0.4 C. It is remarkable that a temperature shift of 20 K up to 313.15 K (40 °C) results in an increase of the specific capacity from 36 mAh g^{-1} to 102 mAh g^{-1} (increase of 183%). On the other hand, a further temperature increase of 20 K results only in a small additional increase of the specific capacity to ~116 mAh g^{-1}. Additionally, a slow damage of the cell is observed, especially if the temperature is enhanced further. Thus, an optimal temperature of the mixtures should be around ~40 °C. Then, even at higher C-rates acceptable capacities are obtained.

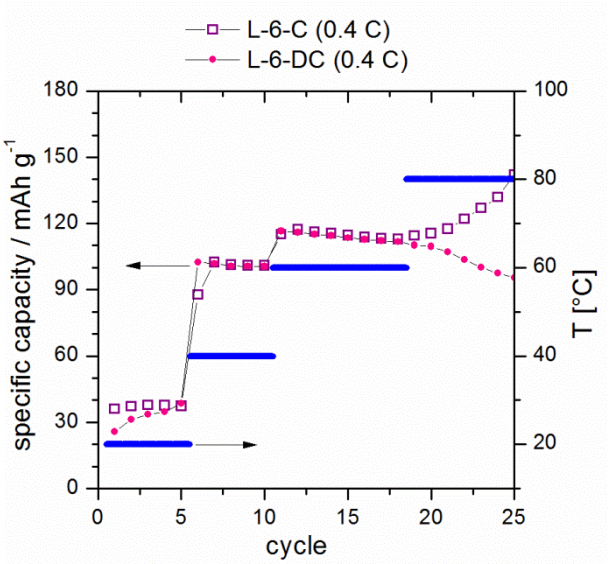

Figure 12. Temperature dependence of the cycling at 0.4 C (= C/2.5). Before the temperature study, the cell was cycled according to Fig 8.

4. CONCLUSION

In this study, selected conducting salts are investigated in a binary electrolyte liquid mixture based on propylene carbonate (PC) and N,N-diethyl-N-methyl-N-(2-methoxyethyl)ammonium bis(trifluoromethanesulfonyl)azanide (DMMA-TFSA). It is shown that the usability of the electrolytes in Li-ion based cells with latest commercially available electrode materials is strongly dependent on the conducting salt. Further it is demonstrated that the ionic liquid DMMA-TFSA which exhibits outstanding properties regarding safety issues and high temperature stability can successfully be used as electrolyte solvent for Li-ion based cells. It is shown that lithium bis(trifluoromethanesulfonyl)azanide (LiTFSA) can be applied in $LiCo_{1/3}Mn_{1/3}Ni_{1/3}O_2$ (NMC)|graphite Li-ion cells for some hundred cycles with an excellent cell performance. Besides the conducting salt, additives play a crucial role in a working cell system. It is found that in mixtures of PC and DMMA-TFSA 2 wt% of vinylene carbonate hampers the PC effectively to exfoliate the graphite layer and enabling a long-term working cell based on graphite and NMC. Further it is proven, that full cell tests are a prerequisite to evaluate the potential of electrolyte mixtures and cell testings against lithium metal are not accurate to conclude electrolyte performances. The results obtained are of broad interest for researchers in different fields of electrochemistry because of the high anodic stability of the electrolytes studied.

ACKNOWLEDGEMENTS
We acknowledge IoLiTec Ionic Liquids Technologies GmbH for kindly providing the ionic liquid DMMA-TFSA. We thank Ralf Heinzmann and Sylvio Indris for performing Lithium diffusion measurements, Martin Tosoni for helpful discussions, and Oliver Schwindt for performing DSC

measurements. We acknowledge support by Deutsche Forschungsgemeinschaft and Open Access Publishing Fund of Karlsruhe Institute of Technology.

References

1. D. Aurbach and O. Chusid, Electrolytes: Additives, in: *Encyclopedia of Electrochemical Power Sources*, Elsevier, Amsterdam, 2009, 92-111.
2. S.S. Zhang, *J. Power Sources*, 162 (2006) 1379-1394.
3. A. Lewandowski, A. Świderska-Mocek, *J. Power Sources*, 194 (2009) 601-609.
4. S. Werner, M. Haumann, P. Wasserscheid, *Annu. Rev. Chem. Biomol. Eng.*, 1 (2010) 203-230.
5. S. Seki, N. Kihira, T. Kobayashi, Y. Kobayashi, Y. Mita, K. Takei, H. Miyashiro, S. Kuwabata, *Electrochemistry*, 77 (2009) 690-692.
6. M. Armand, F. Endres, D.R. MacFarlane, H. Ohno, B. Scrosati, *Nat. Mater.*, 8 (2009) 621-629.
7. A.K. Shukla, T.P. Kumar, *Curr. Sci.*, 94 (2008) 314-331.
8. A. Guerfi, M. Dontigny, P. Charest, M. Petitclerc, M. Lagacé, A. Vijh, K. Zaghib, *J. Power Sources*, 195 (2010) 845-852.
9. A. Chagnes, M. Diaw, B. Carre, P. Willmann, D. Lemordant, *J. Power Sources*, 145 (2005) 82-88.
10. R.S. Kühnel, N. Böckenfeld, S. Passerini, M. Winter, A. Balducci, *Electrochim. Acta*, 56 (2011) 4092-4099.
11. H.F. Xiang, B. Yin, H. Wang, H.W. Lin, X.W. Ge, S. Xie, C.H. Chen, *Electrochim. Acta*, 55 (2010) 5204-5209.
12. T. Sato, T. Maruo, S. Marukane, K. Takagi, *J. Power Sources*, 138 (2004) 253-261.
13. Q.-G. Zhang, S.-S. Sun, S. Pitula, Q.-S. Liu, U. Welz-Biermann, J.-J. Zhang, *J. Chem. Eng. Data*, 56 (2011) 4659-4664.
14. H. Ye, J. Huang, J.J. Xu, A. Khalfan, S.G. Greenbaum, *J. Electrochem. Soc.*, 154 (2007) A1048-A1057.
15. K. Xu, *Chem. Rev.*, 104 (2004) 4303-4417.
16. M. Ue, M. Takeda, M. Takehara, S. Mori, *J. Electrochem. Soc.*, 144 (1997) 2684-2688.
17. R. Jasinski, S. Carroll, *J. Electrochem. Soc.*, 117 (1970) 218-219.
18. H. Yang, K. Kwon, T.M. Devine, J.W. Evans, *J. Electrochem. Soc.*, 147 (2000) 4399-4407.
19. G.H. Lane, A.S. Best, D.R. MacFarlane, M. Forsyth, P.M. Bayley, A.F. Hollenkamp, *Electrochim. Acta*, 55 (2010) 8947-8952.
20. M.L.P. Le, F. Alloin, P. Strobel, J.-C. Leprétre, C.P. Valle, J. P., J. Phys. Chem. B 114 (2010) 894–903.
21. K. Xu, *Energies*, 3 (2010) 135-154.
22. G.J. Wilson, A.F. Hollenkamp, A.G. Pandolfo, *Chem. Int.*, 29 (2007) 16-18.
23. V. Borgel, E. Markevich, D. Aurbach, G. Semrau, M. Schmidt, *J. Power Sources*, 189 (2009) 331-336.
24. T. Matsui, M. Deguchi, H. Yoshizawa, Proc. Meeting Abstracts - 205th Meeting of The Electrochemical Society, MA 2004 01., San Antonio, TX, United States, 2004.
25. M. Pascaly, A. Prodi-Schwab, M. Holzapfel, P. Novak, Proc. 231st ACS National Meeting, Atlanta, March 26-30, 2006.
26. J. Salminen, J.M. Prausnitz, J. Newman, *ECS Transactions*, 1 (2006) 107-118.
27. J. Dong, Z. Zhang, Y. Kusachi, K. Amine, *J. Power Sources*, 196 (2011) 2255-2259.
28. A. Lex-Balducci, R. Schmitz, R.W. Schmitz, R.A. Muller, M. Amereller, D. Moosbauer, H.J. Gores, M. Winter, *ECS Transactions*, 25 (2010) 13-17.
29. N. Yabuuchi, Y. Makimura, T. Ohzuku, *J. Electrochem. Soc.*, 154 (2007) A314-A321.
30. S.-L. Wu, W. Zhang, X. Song, A.K. Shukla, G. Liu, V. Battaglia, V. Srinivasan, *J. Electrochem. Soc.*, 159 (2012) A438-A444.

31. D. Aurbach, B. Gamolsky, B. Markovsky, Y. Gofer, M. Schmidt, U. Heider, *Electrochim. Acta*, 47 (2002) 1423–1439.
32. D. Aurbach, J.S. Gnanaraj, W. Geissler, M. Schmidt, *J. Electrochem. Soc.*, 151 (2004) A23-A30.
33. L. El Ouatani, R. Dedryvere, C. Siret, P. Biensan, D. Gonbeau, *J. Electrochem. Soc.*, 156 (2009) A468-A477.
34. L. El Ouatani, R. Dedryvere, C. Siret, P. Biensan, S. Reynaud, P. Iratcabal, D. Gonbeau, *J. Electrochem. Soc.*, 156 (2009) A103-A113.
35. J.-Y. Eom, I.-H. Jung, J.-H. Lee, *J. Power Sources*, 196 (2011) 9810-9814.
36. D. Linden, T.B. Reddy, Handbook of Batteries, Third ed., McGraw-Hill, 2001.
37. M. Dahbi, F. Ghamouss, F. Tran-Van, D. Lemordant, M. Anouti, *J. Power Sources*, 196 (2011) 9743-9750.
38. Y. Jin, S. Fang, L. Yang, S.-i. Hirano, K. Tachibana, *J. Power Sources*, 196 (2011) 10658-10666.
39. H. Vogel, *Phys. Z.*, 22 (1921) 645.
40. G.S. Fulcher, *J. Am. Ceram. Soc.*, 8 (1925) 339.
41. G. Tammann, W. Hesse, *Z. Anorg. Allg. Chem.*, 156 (1926) 245.
42. C. Schreiner, S. Zugmann, R. Hartl, H.J. Gores, *J. Chem. Eng. Data* 55 (2010) 4372-4377.
43. W. Xu, E.I. Cooper, C.A. Angell, *J. Phys. Chem. B*, 107 (2003) 6170-6178.
44. C.A. Angell, *Science*, 267 (1995) 1924-1935.
45. C.A. Angell, W. Xu, M. Yoshizawa, A. Hayashi, J.-P. Belieres, P. Lucas, M. Videa, Physical Chemistry of Ionic Liquids, Inorganic and Organic, Protic and Aprotic, in: H. Ohno (Ed.) Electrochemical aspects of ionic liquids, John Wiley & Sons, 2005, pp. 5-23.
46. M.L.F. Nascimento, C. Aparicio, *Physica B*, 398 (2007) 71-77.
47. C. Schreiner, S. Zugmann, R. Hartl, H.J. Gores, *J. Chem. Eng. Data* 55 (2009) 1784-1788.
48. K.R. Harris, M. Kanakubo, L.A. Woolf, *J. Chem. Eng. Data*, 52 (2007) 1080-1085.
49. The parameter m was calculated according to equation (10) in literature C. Schreiner, S. Zugmann, R. Hartl and H. J. Gores, *J. Chem. Eng. Data*, 2010, *55*, 4372.
50. R. Zarrougui, M. Dhahbi, D. Lemordant, *J. Sol. Chem.*, 39 (2010) 921-942.
51. T. Frömling, M. Kunze, M. Schönhoff, J. Sundermeyer, B. Roling, *J. Phys. Chem. B* 112 (2008) 12985–12990.
52. P. Walden, *Z. Phys. Chem.*, 55 (1906) 207-246.
53. D. Aurbach, A. Zaban, Y. Ein-Eli, I. Weissman, O. Chusid, B. Markovsky, M. Levi, E. Levi, A. Schechter, E. Granot, *J. Power Sources*, 68 (1997) 91-98.
54. D. Aurbach, M.D. Levi, E. Levi, A. Schechter, *J. Phys. Chem. B*, 101 (1997) 2195-2206.
55. D.P. Abraham, M.M. Furczon, S.H. Kang, D.W. Dees, A.N. Jansen, *J. Power Sources*, 180 (2008) 612-620.
56. A.P. Lewandowski, A.F. Hollenkamp, S.W. Donne, A.S. Best, *J. Power Sources*, 195 (2010) 2029-2035.